Numerical analysis for radiation-resistant GaAs heteroface solar cell structures

Masafumi Yamaguchi and Chikara Amano
Ibaraki Electrical Communication Laboratory, Nippon Telegraph and Telephone Public Corporation, Tokai, Ibaraki-ken 319-11, Japan

(Received 7 May 1984; accepted for publication 6 July 1984)

Experimental studies and numerical analyses are carried out to optimize A1GaAs-GaAs heteroface solar cell structures. Carrier removal rate and damage constant for diffusion length in n-GaAs due to 1-MeV electron irradiation are found to be larger than those in p-GaAs. These results are explained by taking into account deep-level traps associated with radiation-induced defects. Numerical analysis shows that n^{++}-n^{+}-p heteroface cell structure is relatively radiation resistant in a shallow junction solar cell (below 0.2 μm) with a substrate carrier concentration above 3×10^{15}cm^{-3}. In the p^{++}-p^{+}-n heteroface solar cell, optimum junction depth and substrate carrier concentration are 0.2–0.3 μm and 2–5$\times10^{15}$ cm^{-3}, while those in the n^{++}-n^{+}-p heteroface solar cell are less than 0.1 μm and 3–10$\times10^{15}$ cm^{-3}.

I. INTRODUCTION

The last few years have seen increasing interest in the use of GaAs for solar cell applications. Recently, A1GaAs-GaAs heteroface solar cells with an air mass zero (AM0) conversion efficiency of 18.5% have been reported by Hovel and Woodall.[1] This high efficiency cell has also shown a good potential for space applications. In a space environment, solar cells are subjected to continual bombardment by electrons, protons, and other particles. Such particles penetrate the semiconductor and cause considerable lattice damage in the form of vacancies, interstitials, and complexes. This radiation damage has an effect on the transport properties of the semiconductor, in particular reducing the carrier concentration, mobility, and lifetime, which results in a gradual deterioration in solar cell performance. Thus, for GaAs solar cells, it is essential to investigate and understand the physical aspects and fundamental limitations of these solar cells under various radiation conditions. Although a handful of reports have dealt with radiation damage in GaAs solar cells,[2–5] optimization of radiation-resistant cell structures in GaAs solar cells has not yet been examined.

The purpose of this paper is to optimize radiation-resistant and high efficiency A1GaAs-GaAs heteroface solar cell structures. 1-MeV electron irradiation damage of GaAs single crystals is first examined, and the relationships between recombination parameters such as carrier diffusion length and carrier concentration, and deep-level trap parameters are clarified. Changes in solar cell properties caused by 1-MeV electron irradiation are analyzed by using recombination parameters. Numerical analyses are then presented for optimizating A1GaAs-GaAs heteroface solar cell structure to tolerate radiation-induced degradation in electronic properties. Numerical analysis shows optimum cell configuration, window layer thickness, junction depth and substrate carrier concentration for radiation-resistant and high efficiency GaAs heteroface solar cell.

II. EXPERIMENTS

The samples used in this work were cut from n-type GaAs single crystals, undoped and doped with Si, having carrier concentrations in the range of 10^{15}–10^{18} cm^{-3} at 300 K, and Schottky diodes or p^{+}-n junction diodes were made by Schottky contact formation or LPE (liquid phase epitaxy). The p^{+} side was doped with Zn in the 10^{18} cm^{-3} range. As shown in Fig. 1(a), A1GaAs-GaAs heteroface solar cells were also used in this study. The cells were fabricated by LPE. Initial carrier concentration values, minority carrier diffusion lengths, and other parameters for the p^{++}-A1GaAs window layer, p^{+}-GaAs diffused layer, and n-GaAs substrate are listed in Table I. Cell area was 0.105 cm^2. SiO deposited to a thickness of about 1000 Å was used as an antireflection (AR) coating. Typical values for the short-circuit current density, open-circuit voltage, and maximum

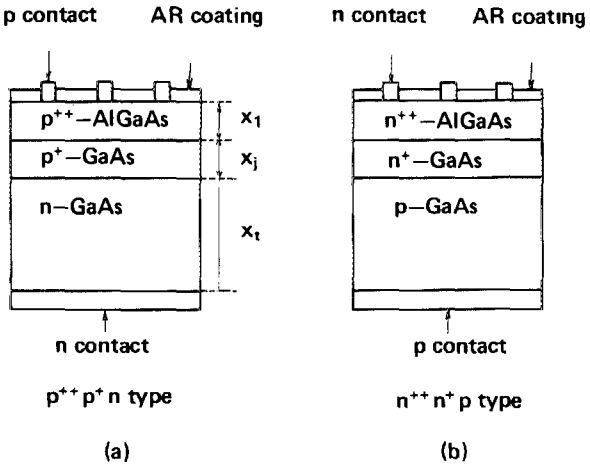

FIG. 1. (a) Diagram of a p^{++}-p^{+}-n A1GaAs-GaAs heteroface solar cell. (b) Diagram of an n^{++}-n^{+}-p A1GaAs-GaAs heteroface solar cell.

 0021-8979/85/020537-08$02.40

TABLE I. Physical parameters for GaAs heteroface solar cell.

Layer	Parameter	Symbol	Value
p^{++}-AlGaAs window layer	carrier concentration	N_{p1}	5×10^{18} cm^{-3}
	electron diffusion length	L_{n1}	3.15 μm
	electron diffusion constant	D_{n1}	5 cm^2/s
	AlAs content	x	0.70
	layer thickness	x_1	1.5 μm
	surface recombination velocity	S	1×10^7 cm/s
p^+-GaAs diffused layer	carrier concentration	N_{p2}	5×10^{18} cm^{-3}
	electron diffusion length	L_{n2}	6.6 μm
	electron diffusion constant	D_{n2}	40 cm^2/s
	junction depth	x_j	3.5 μm
n-GaAs substrate	carrier concentration	N_n	5×10^{17} cm^{-3}
	hole diffusion length	L_p	4.73 μm
	hole diffusion constant	D_p	5 cm^2/s
	substrate thickness	x_s	250 μm

power density before irradiation were 24.3 mA/cm^2, 0.985 V, and 18.3 mW/cm^2 under an AM1.5 illumination of 100 mW/cm^2.

1-MeV electron irradiation was carried out using a Cockcroft–Walton electron accelerator at room temperature. Electron flux density below 10^{12} cm^{-2}s^{-1}, low enough to avoid sample heating, was used up to maximum fluence of 3×10^{15} cm^{-2}.

The minority carrier diffusion lengths for n and p^+ layers and the carrier concentrations in n layer were determined using SEM-EBIC method and C-V measurements. Solar cell I-V curves before and after irradiation were measured using an AM 1.5 solar simulator as the light source. All measurements were taken at 300 K.

III. RESULTS AND DISCUSSION

A. Relationship between changes in minority carrier diffusion lengths and carrier concentrations with irradiation and radiation-induced deep-level traps

In order to clarify the effect of radiation on GaAs cell material, the relationship between electrical property changes with irradiation and radiation-induced deep-level traps was examined.

Figure 2 shows changes in carrier removal Δn for n-type GaAs with various initial carrier concentrations as a function of 1-MeV electron irradiation fluence. This figure suggests that the carrier removal rate R_c ($=\Delta n/\phi$) for electron-irradiated n-GaAs depends on the initial carrier con-

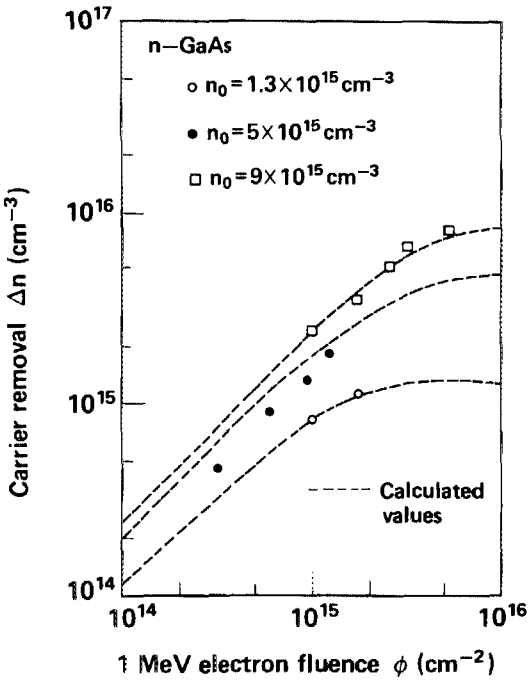

FIG. 2. Changes in carrier removal Δn for n-GaAs with various initial carrier concentrations as a function of 1-MeV electron irradiation fluence. The dashed lines show calculated values taking into account radiation-induced deep-level majority-carrier traps.

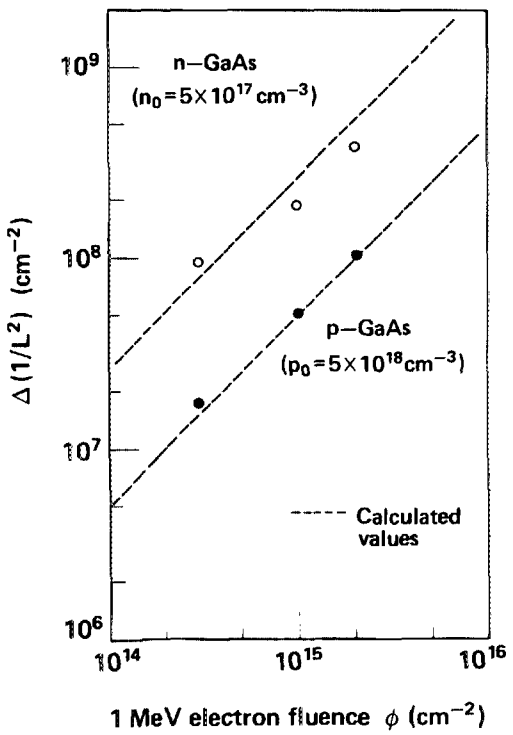

FIG. 3. Changes in inverse square of diffusion length Δ ($1/L^2$), for p-GaAs ($p_0=5\times10^{18}$ cm^{-3}) and n-GaAs ($n_0=5\times10^{17}$ cm^{-3}) as a function of 1-MeV electron irradiation fluence. The dashed lines show the calculated values.

centration, that is, it depends on the position of the Fermi level. However, this figure does not imply that impurity effects play a role in the carrier removal rate for GaAs, because the experimental data in Fig. 2 are in good agreement with the theoretical values, calculated under the assumption that the radiation-induced defect introduction rate does not vary with impurity species and concentration.

Figure 3 shows changes in the inverse square of diffusion length $\Delta(1/L^2)$, for p-GaAs ($p_0 = 5\times10^{18}$ cm^{-3}) and n-GaAs ($n_0 = 5\times10^{17}$ cm^{-3}) as a function of 1-MeV electron fluence. It can be seen from Fig. 3 that damage constant $K_L[=\Delta(1/L^2)/\phi]$ for n-GaAs is larger than that for p-GaAs. In this figure, the experimental results for diffusion length are also seen to be in good agreement with the dashed-line curves for the theoretical values, calculated under the assumption that the radiation-induced defect introduction rate does not depend on impurity species and concentration.

In order to clarify the effects on initial carrier concentration and conductivity type on the carrier removal rate and damage constant in GaAs, calculated values for these quantities were compared with the experimental results.

Carrier removal rate R_c in GaAs due to irradiation was assumed to be

$$R_c = \sum I_{t_i} f(E_{t_i}), \tag{1}$$

$$f(E_{t_i}) = 1/\{1 + 2\exp[(E_{t_i} - E_F)/kT]\}, \tag{2}$$

where I_{t_i} is the introduction rate of the ith defect level, $f(E_{t_i})$ is the carrier trapping rate due to trap level E_{t_i} and E_F is the Fermi level. The Fermi level E_F is given by the condition of charge neutrality as follows:

$$n + \phi\sum I_{t_a} f(E_{t_a}) = p + \phi\sum I_{t_d} f(E_{t_d}) + N_D - N_A, \tag{3}$$

where ϕ is integrated fluence and the subscripts a and d refer to the defect acceptor and donor centers, respectively.

Damage constant K_L for minority carrier diffusion length due to irradiation was assumed to be as follows:

$$\Delta(1/L^2) = 1/L_\phi^2 - 1/L_0^2 = K_L\phi, \tag{4}$$

$$K_L = \sum I_{t_j}\tau_j f(E_{t_j})v/D, \tag{5}$$

TABLE II. Energy levels, capture cross sections, and introduction rates of deep levels in GaAs by 1-MeV electron irradiation used in analysis.

Trap	Energy level E_t (eV)	Capture cross section σ (cm^2)	Introduction rate I_t(cm^{-1})
$E1$	$E_c - 0.08$	$\sigma_n = 10^{-17}$	1.8
$E2$	$E_c - 0.14$	$\sigma_n = 1.2\times10^{-15}$	2.8
$E3$	$E_c - 0.35$	$\sigma_n = 6.2\times10^{-15}$	0.3
$E4$	$E_c - 0.71$	$\sigma_n = 2.2\times10^{-13}$	0.07
$E5$	$E_c - 0.90$	$\sigma_n = 5.8\times10^{-14}$	0.1
$H1$	$E_v + 0.13$	$\sigma_p = 5.9\times10^{-18}$	0.22
$H2$	$E_v + 0.29$	$\sigma_p = 5.9\times10^{-18}$	0.7
$H3$	$E_v + 0.35$		0.08
$H4$	$E_v + 0.44$	$\sigma_p = 9\times10^{-15}$	0.4
$H5$	$E_v + 0.71$	$\sigma_p = 2.3\times10^{-13}$	0.4

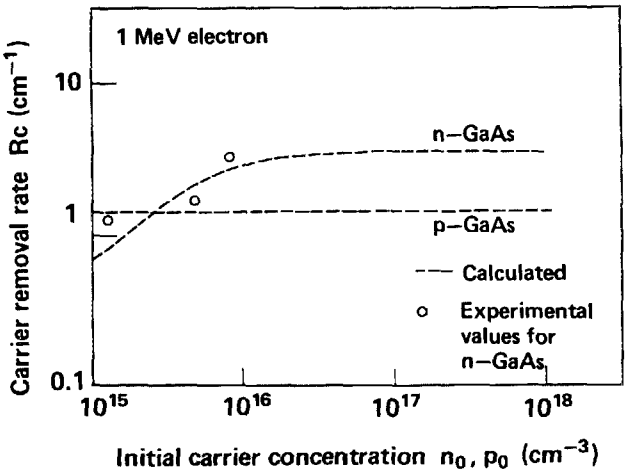

FIG. 4. Calculated carrier removal rate R_c in 1-MeV electron irradiated n-GaAs and p-GaAs vs initial carrier concentration. Experimental data for carrier removal rate in n-GaAs are shown by open circles.

$$\left.\begin{aligned} f(E_{t_j}) &= \exp[(E_F - E_{t_j})/kT], \quad E_F < E_{t_j} \\ f(E_{t_j}) &= 1, \qquad\qquad\qquad E_F > E_{t_j} \end{aligned}\right\} \tag{6}$$

where L_0 and L_ϕ are minority carrier diffusion length before and after irradiation, respectively, I_{t_j} is the introduction rate of the jth defect level, $f(E_{t_j})$ represents the probability that the jth defect level E_{t_j} will capture a minority carrier, σ_j is the cross section for minority-carrier capture by the jth defect center, v is the thermal velocity of minority carriers, and D is the minority carrier diffusion coefficient.

Table II shows the energy levels, capture cross sections and introduction rates of deep levels in GaAs by 1-MeV electron irradiation used in analysis. This table shows a summary of DLTS data for 1-MeV electron irradiated GaAs reported by Lang *et al.*,[6] Pons *et al.*,[7] and Li *et al.*[8] Carrier removal rates and damage constants in n-GaAs and p-GaAs were assumed to be influenced by five deep electron and hole traps shown in Table II. According to the reference data,[9–12] the diffusion coefficients for electron and hole D_n, D_p (cm^2/s) were assumed to be expressed by the following relations:

$$D_n = 1.232\times10^8/(5.793\times10^5 + N_p^{1/3}) \tag{7}$$

$$D_p = 7.347\times10^6/(6.697\times10^5 + N_n^{1/3}) \tag{8}$$

where N_n, N_p are hole and electron concentrations (cm^{-3}), respectively.

Figure 4 shows calculated carrier removal rate in 1-MeV electron irradiated n-GaAs and p-GaAs versus initial carrier concentration. In this figure, the experimental data for the carrier removal rate in n-GaAs are also shown in comparison. It can be seen in Fig. 4 that the carrier removal rate for n-GaAs is greater than that for p-GaAs, and that the carrier removal rate for n-GaAs has a somewhat stronger carrier concentration dependence. These results can be explained by a large total introduction rate for electron traps and shallow levels of electron traps with large introduction rates.

Figure 5 shows calculated damage constants for diffusion length in 1-MeV electron irradiated n-GaAs and p-

GaAs versus initial carrier concentration compared with the experimental data. It can be seen from Fig. 5 that the damage constant for diffusion length K_L for n-GaAs is larger than that for p-GaAs.

As shown in Figs. 2–5, the calculated values for carrier removal and diffusion length changes in GaAs due to irradiation are in good agreement with the experimental data. It is therefore concluded that electron-induced carrier removal and diffusion length changes in GaAs, and initial carrier concentration and conductivity-type effects on them can be expressed by the equations taking into account deep-level traps associated with radiation-induced defects whose introduction rate was assumed to be independent of impurity species and concentration.

B. Experimental results for solar cell property change with irradiation and numerical analysis on solar cell irradiation damage

Computed results for heteroface solar cell irradiation damage are compared with the experimental results obtained with 1-MeV electron irradiation at room temperature.

Figure 6 shows an illustration of the band profile model for the A1GaAs-GaAs heteroface solar cell used in analysis. In these calculations, solar cell surface reflection loss was ignored.

The photogenerated electron density J_n in the p layer is given by[13]

$$J_n = qF\alpha_2 L_{n2}/(1-\alpha_2^2 L_{n2}^2) \times \exp(-\alpha_1 x_1)\times\{<\tanh(x_j/L_{n2})+\alpha_2 L_{n2}> \times\exp(-\alpha_2 x_j)-\alpha_2 L_{n2}/\cosh(x_j/L_{n2})\} + j_0/\cosh(x_j/L_{n2}). \quad (9)$$

Here, j_0 is electron current density, which is injected from the window (I) layer to the p^+-GaAs (II) layer and is given by

$$j_0 = qF\alpha_1 L_{n1}/(1-\alpha_1^2 L_{n1}^2)\{\{[\tanh(x_j/L_{n1}) + L_{n1}S/D_{n1}]/[1+\tanh(x_1/L_{n1})L_{n1}S/D_{n1}] + \alpha_1 L_{n1}\}\exp(-\alpha_1 x_1) - (\alpha_1 L_{n1} + L_{n1}S/D_{n1})/[\cosh(x_1/L_{n1}) + (L_{n1}S/D_{n1})\sinh(x_1/L_{n1})]\}, \quad (10)$$

where suffixes 1 and 2 show regions I and II, respectively, x_1 and x_j are window-layer thickness and junction depth, F is photon flux, α is absorption coefficient, S is surface recombination velocity, and D is the diffusion coefficient for minority carriers.

The photogenerated current density collected from the depletion region is

$$J_d = qF[1-\exp(-\alpha_2 W)]\exp(-\alpha_1 x_1 - \alpha_2 x_j), \quad (11)$$

where W is the width of the depletion layer.

The photogenerated hole current density J_p in an n-type layer is given by

$$J_p = qF\alpha_2 L_p/(1+\alpha_2 L_p)\exp(-\alpha_1 x_1 - \alpha_2 x_j - \alpha_2 W). \quad (12)$$

The total current density delivered by the cell is expressed by

$$J_{sc} = J_n + J_d + J_p. \quad (13)$$

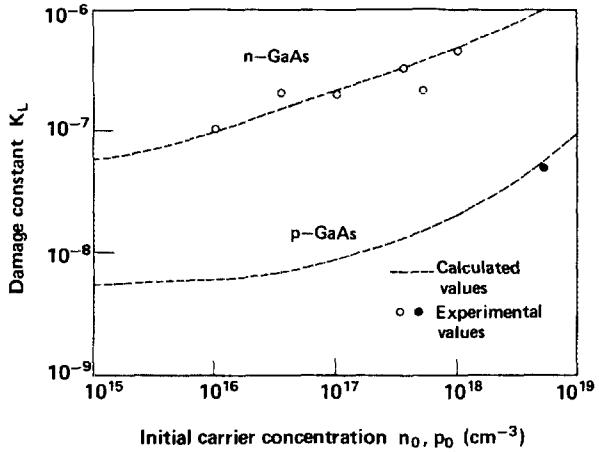

FIG. 5. Calculated damage constant K_L for minority carrier diffusion length in 1-MeV electron irradiated n-GaAs and p-GaAs vs initial carrier concentration compared with experimental data for n-GaAs (open circles) and p-GaAs (closed circles).

The open-circuit voltage V_{oc} is given by

$$V_{oc} = (nkT/q)\ln[(I_{sc}/I_0)+1]. \quad (14)$$

The maximum current I_m at the maximum power point can be determined as a solution of the following equation:

$$\ln[(I_{sc}-I_m)/I_0] - 2qI_m R_s/(nkT) = I_m/(I_{sc}-I_m), \quad (15)$$

where R_s is the total series resistance for the solar cell. Power conversion efficiency η at the maximum power point is

$$\eta = V_m I_m / P_{in}, \quad (16)$$

and fill factor FF is

$$FF = V_m I_m/(V_{oc} I_{sc}), \quad (17)$$

where P_{in} is input light power.

Three band edges (eV), $E_{\Gamma 1}$, E_{x1}, and $E_{\Gamma 15}$ for $Al_x Ga_{1-x}As$ and GaAs were assumed to influence optical absorption[14]:

$$E_{\Gamma 1} = 1.44 + 1.04x + 0.47x^2, \quad (18)$$

$$E_{x1} = 1.92 + 0.17x + 0.07x^2, \quad (19)$$

$$E_{\Gamma 15} = 2.90 + 0.36x + 0.54x^2. \quad (20)$$

Absorption coefficients α for energy near, but larger than, their respective band edges are empirically expressed by[15]

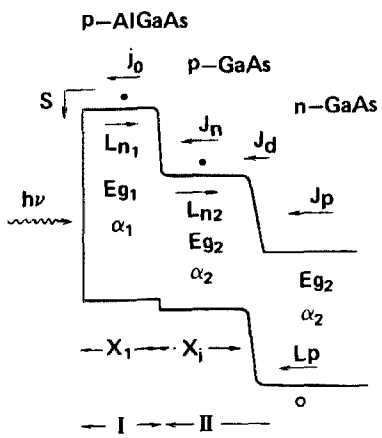

FIG. 6. Band profile mode illustration for an A1GaAs-GaAs heteroface solar cell used in analysis.

$$\alpha_{\Gamma 1} = 4.0\times 10^4 (h\nu - E_{\Gamma 1})^{1/2}\ (\mathrm{cm}^{-1}), \tag{21}$$

$$\alpha_{x1} = 1.0\times 10^3 (h\nu - E_{x1})^{2}\ (\mathrm{cm}^{-1}), \tag{22}$$

$$\alpha_{\Gamma 15} = 3.5\times 10^5 (h\nu - E_{\Gamma 15})^{1/2}\ (\mathrm{cm}^{-1}), \tag{23}$$

where $h\nu$ is photon energy (eV).

The solar cell damage was assumed to be due to the decrease in minority carrier diffusion lengths and carrier concentration in each layer. The point defects were assumed to be uniformly introduced in the cell by electron irradiation. Carrier concentration and minority carrier diffusion length changes due to irradiation were assumed to be expressed by Eqs. (1)–(3) and (1)–(6), repectively. These parameter changes in the p^{++}-AlGaAs layer with irradiation were assumed to be the same as those in p^{+}-GaAs layer.

Table I shows the physical parameters for the AlGaAs-GaAs heteroface solar cells used in the analysis.

Figure 7 shows theoretical fitting to the experimental degradation values for power conversion efficiency η_ϕ/η_0 at AM1.5 by 1-MeV electron irradiation. Good agreement with the experimental results was obtained. Such excellent agreement implies the adequacy of the model and pertinent assumptions. Solar cell damage due to electron irradiations is concluded to be mainly due to decreases in minority carrier diffusion lengths and carrier concentrations.

Therefore, it is concluded that GaAs solar cell damage can be evaluated by using irradiation damage data for GaAs single crystals, that is, using minority carrier diffusion lengths and carrier concentration data, or deep-level trap data in GaAs.

C. Optimization of the GaAs heteroface solar cell structure

In this section, the numerical analysis results for optimization of the AlGaAs-GaAs heteroface solar cell structure will be discussed. The n^{++}-n^{+}-p heteroface cell shown in Fig. 1(b) was also analyzed as well as the p^{++}-p^{+}-n heteroface cell [Fig. 1(a)], by modifying Eqs. (9)–(12). In these calculations, the aluminum content x in the $Al_xGa_{1-x}As$ window layer was taken to be 0.9 and the window layer thickness was taken to be 0.1 μm. According to the reference data,[16] the initial minority carrier diffusion lengths L_{n0}, L_{p0} (cm) were assumed to be expressed by the following relations:

$$L_{n0} = 1.26\times 10^3 N_{p0}^{-1/3}, \tag{24}$$

$$L_{p0} = 13.9 N_{n0}^{-1/4}. \tag{25}$$

Carrier diffusion coefficients were assumed to follow from Eqs. (7) and (8), and surface recombination velocity in the window layer was assumed to be 1×10^7 cm/s. Carrier concentration and minority carrier diffusion length changes due to irradiation were assumed to be expressed by Eqs. (1)–(3), and Eqs. (1)–(6), respectively.

1. Optimization of window layer thickness

Figure 8 shows calculated AM0 conversion efficiency versus AlGaAs window layer thickness for p^{++}-p^{+}-n heteroface solar cells with a junction depth of 0.1 μm and a substrate carrier concentration of 1×10^{16} cm^{-3} as a function of 1-MeV electron fluence. Numerical analysis shows that conversion efficiency of the heteroface solar cell increases with decreases in window layer thickness. In practice, undulations at small AlGaAs thickness are expected to be caused by optical interference[17] in AlGaAs and AR coating films. However, the optimum window layer thickness for high efficiency heteroface solar cells is thought to be about 0.1 μm.

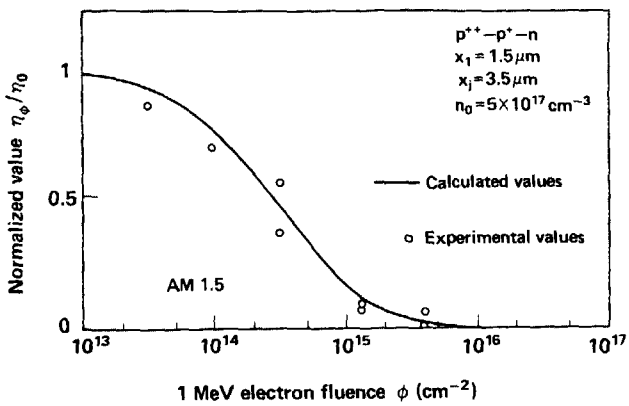

FIG. 7. Theoretical fitting to experimental values of power conversion efficiency η_ϕ/η_0 degradation by 1-MeV electron irradiation.

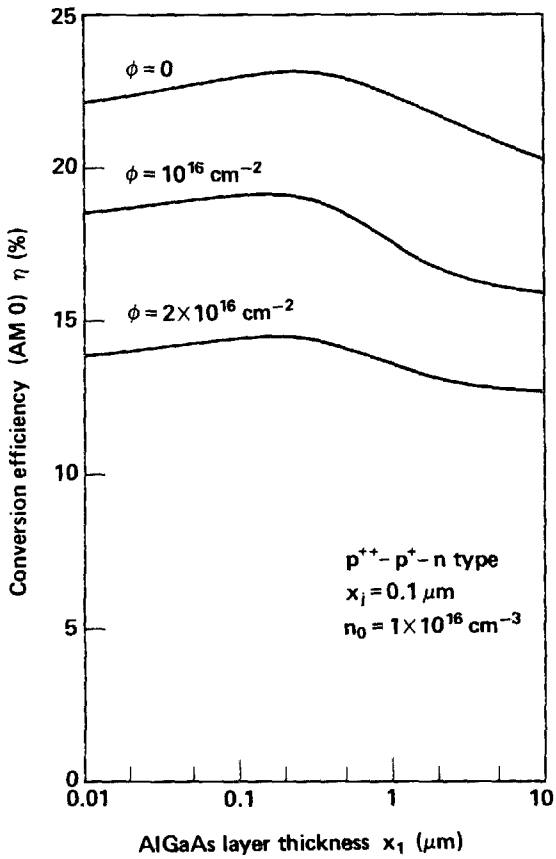

FIG. 8. Calculated AM0 conversion efficiency vs AlGaAs window layer thickness for a p^{++}-p^{+}-n heteroface solar cell with a junction depth of 0.1 μm and a substrate carrier concentration of 1×10^{16} cm^{-3} as a function of 1-MeV electron fluence.

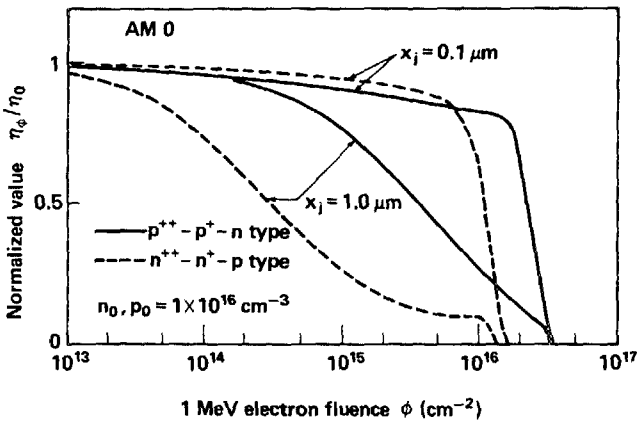

FIG. 9. Calculated AM0 power conversion efficiency changes with 1-MeV electron fluence for p^{++}-p^+-n (solid lines) and n^{++}-n^+-p (dashed lines) AlGaAs-GaAs heteroface solar cells with various junction depths and a substrate carrier concentration of $1\times10^{16}\ cm^{-3}$.

2. Optimization of cell configuration

Figure 9 shows calculated AM0 power conversion efficiency changes due to 1-MeV electron fluence, for p^{++}-p^+-n and n^{++}-n^+-p AlGaAs-GaAs heteroface solar cells with various junction depths and a substrate carrier concentration of $1\times10^{16}\ cm^{-3}$. It can be seen from Fig. 9 that a shal-junction solar cell should be more radiation resistant than a deep junction solar cell. Moreover, in a shallow junction solar cell (for example, $x_j = 0.1\ \mu m$], the n^{++}-n^+-p cell structure is found to be more radiation resistant than the p^{++}-p^+-n cell, while the p^{++}-p^+-n cell structure is more radiation resistant than the n^{++}-n^+-p structure in a deep junction solar cell (for example, $x_j = 1\mu m$).

As described above, deterioration of diffusion length in n-GaAs is greater than that in p-GaAs. Therefore, the n^{++}-n^+-p cell structure with p-GaAs substrate should be relatively radiation resistant in a shallow junction solar cell, because, in a shallow junction cell, photogenerated carriers are mainly collected in the substrate layer. On the other hand, in a deep junction solar cell, p^{++}-p^+-n cell structure with p^+-GaAs diffused layer should be relatively radiation resistant, because photogenerated carriers are mainly collected in the surface diffused layer.

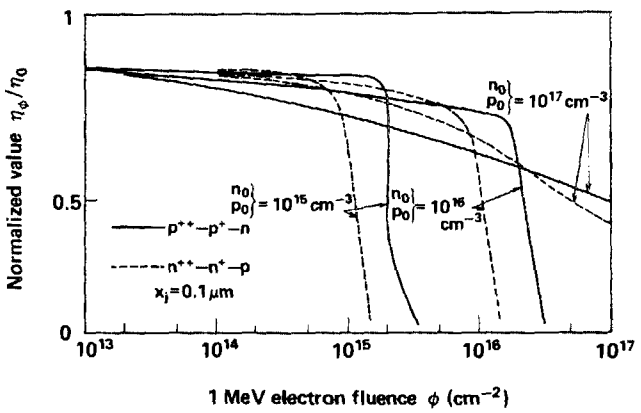

FIG. 10. Calculated AM0 power conversion efficiency changes with 1-MeV electron fluence for p^{++}-p^+-n (solid lines) and n^{++}-n^+-p (dashed lines) AlGaAs-GaAs heteroface solar cells with various substrate carrier concentrations and a junction depth of 0.1 μm.

Figure 10 shows calculated AM0 power conversion efficiency changes due to 1-MeV electron fluence for GaAs p^{++}-p^+-n and n^{++}-n^+-p heteroface solar cells with various carrier concentrations and a junction depth of 0.1 μm. In a low irradiation fluence, a solar cell with a low carrier concentration substrate is relatively radiation tolerant, because low carrier concentration GaAs has a low damage constant of diffusion length. On the other hand, in a high irradiation fluence, a solar cell with a low carrier concentration substrate experiences relatively severe deterioration of power conversion efficiency, because low carrier concentration substrates are greatly influenced by increases in series resistance due to decreases in carrier concentration following irradiation.

Moreover, it can be seen from Fig. 10 that in a cell with a high carrier concentration substrate (above $10^{16}\ cm^{-3}$), n^{++}-n^+-p cell structure is more radiation resistant than p^{++}-p^+-n structure, while in a cell with a low carrier concentration substrate (below $10^{15}\ cm^{-3}$), p^{++}-p^+-n cell structure is relatively radiation resistant. In the cell with a high carrier concentration substrate, because conversion efficiency degradation is mainly due to a decrease in diffusion length, the n^{++}-n^+-p with p-GaAs substrate is relatively radiation tolerant. On the other hand, in the cell with a low carrier concentration substrate, the p^{++}-p^+-n with n-GaAs substrate is relatively radiation resistant, because conversion efficiency degradation is mainly due to decreases in carrier concentration, and high mobility GaAs has low series resistance.

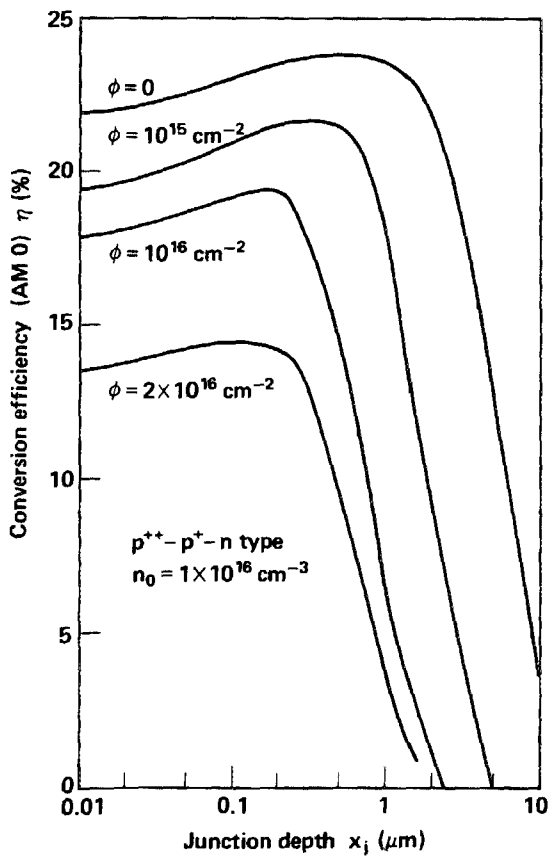

FIG. 11. Calculated AM0 conversion efficiency vs junction depth for a p^{++}-p^+-n heteroface solar cell with a substrate carrier concentration of $1\times10^{16}\ cm^{-3}$ as a function of 1-MeV electron fluence.

Therefore, it is concluded that n^{++}-n^{+}-p heteroface cell structure yields high efficiency and radiation-resistant cells with shallow junction below 0.2 μm and substrate carrier concentrations above 3×10^{15} cm^{-3}. On the other hand, p^{++}-p^{+}-n heteroface cell structure is relatively radiation resistant with deep junctions above 0.2 μm and low substrate carrier concentrations below 3×10^{15} cm^{-3}.

3. Optimization of junction depth

Figure 11 shows calculated AM0 conversion efficiency versus junction depth for a p^{++}-p^{+}-n heteroface solar cell with a substrate carrier concentration of 1×10^{16} cm^{-3} as a function of 1-MeV electron fluence. Optimum junction depth for a high efficiency, radiation-resistant p^{++}-p^{+}-n heteroface cell becomes shallower as irradiation fluence increases. A junction depth x_j of 0.5 μm is optimum for an initial high efficiency cell, because in the p^{++}-p^{+}-n heteroface cell, collecting photogenerated carriers with large diffusion lengths in the p^{+}-GaAs layer results in high cell efficiency. A junction depth of 0.2–0.3 μm is optimum for high efficiency, radiation-resistant cell.

Figure 12 shows calculated AM0 conversion efficiency versus junction depth for an n^{++}-n^{+}-p heteroface solar cell with a substrate carrier concentration of 1×10^{16} cm^{-3}as a function of 1-MeV electron fluence. In n^{++}-n^{+}-p heteroface solar cells, collecting photogenerated carriers with large diffusion length in the p-GaAs substrate layer is useful for a high efficiency solar cell. Thus, for an initial high efficiency

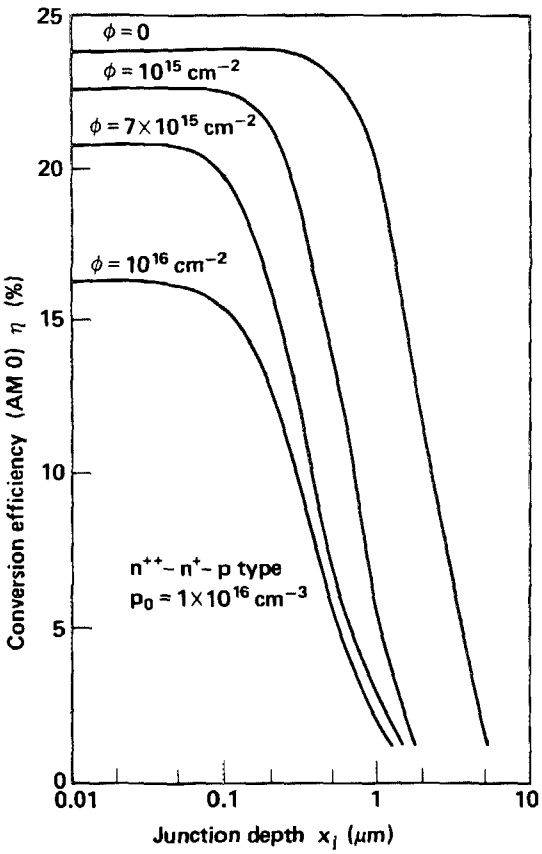

FIG. 12. Calculated AM0 conversion efficiency vs junction depth for an n^{++}-n^{+}-p heteroface solar cell with a substrate carrier concentration of 1×10^{16} cm^{-3} as a function of 1-MeV electron fluence.

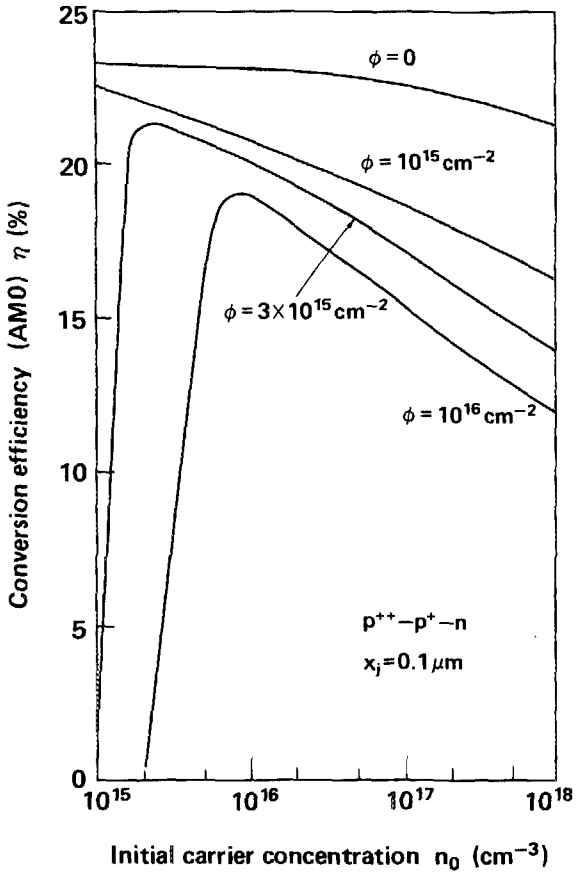

FIG. 13. Calculated AM0 conversion efficiency vs initial substrate carrier concentration for a p^{++}-p^{+}-n heteroface solar cell with a junction depth of 0.1 μm as a function of 1-MeV electron fluence.

cell, a junction depth of x_j about 0.2 μm is optimum. Optimum junction depth for high efficiency and radiation-resistant n^{++}-n^{+}-p heteroface cells also becomes shallower as irradiation fluence increases. Following irradiation with $(1–10)\times10^{15}$ cm^{-3}, a junction depth x_j less than 0.1 μm was found to be optimum.

Therefore, it is concluded that optimum junction depths for radiation-resistant p^{++}-p^{+}-n and n^{++}-n^{+}-p heteroface solar cells are 0.2–0.3 μm and less than 0.1 μm, respectively.

4. Optimization of substrate carrier concentration

Figure 13 shows calculated AM0 conversion efficiency versus initial substrate carrier concentration for p^{++}-p^{+}-n heteroface solar cells with a junction depth of 0.1 μm as a function of 1-MeV electron fluence. Before irradiation, solar cells with low substrate carrier concentrations exhibited high efficiency because low carrier concentration substrates offer large diffusion length and collecting effect of photogenerated carriers from the depletion region. However, optimum substrate carrier concentration becomes higher as irradiation proceeds, because conversion efficiency degradation is mainly due to decreasing carrier concentrations in high irradiation fluence. The optimum substrate carrier concentration for radiation-resistant solar cells is found to be $(2–5)\times10^{15}$ cm^{-3}.

Figure 14 shows calculated AM0 conversion efficiency versus initial substrate carrier concentration for n^{++}-n^{+}-p

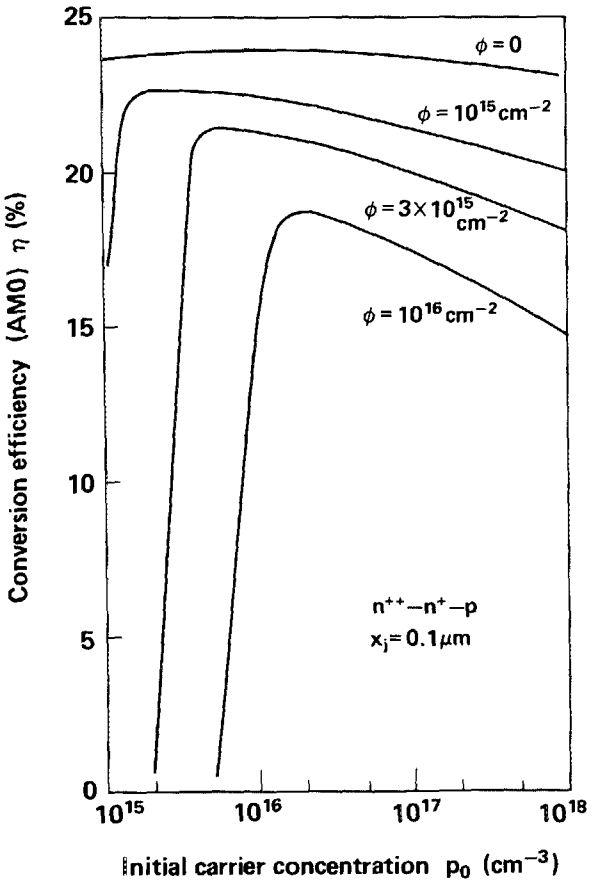

FIG. 14. Calculated AM0 conversion efficiency vs initial substrate carrier concentration for an n^{++}-n^{+}-p heteroface solar cell with a junction depth of 0.1 μm as a function of 1-MeV electron fluence.

heteroface solar cells with a junction depth of 0.1 μm as a function of 1-MeV electron fluence. Similar to the p^{++}-p^{+}-n cell, the optimum substrate carrier concentration in the n^{++}-n^{+}-p cell structure becomes higher as irradiation proceeds. The optimum substrate carrier concentration for radiation-resistant solar cells is found to be $(3\text{–}10)\times10^{15}$ cm^{-3}.

Therefore, it is concluded that the optimum substrate carrier concentration for radiation-resistant p^{++}-p^{+}-n and n^{++}-n^{+}-p heteroface solar cells is $(2\text{–}5)\times10^{15}$ and $(3\text{–}10)\times10^{15}$ cm^{-3}, respectively.

IV. CONCLUSION

Experimental studies and numerical analyses have been carried out to optimize AlGaAs-GaAs heteroface solar cell structures. The following conclusions have been derived from the present investigations.

(1) Carrier removal and diffusion length changes due to 1-MeV electron irradiation in GaAs have been studied. Carrier removal rates and damage constants for diffusion lengths in n-GaAs are found to be larger than those in p-GaAs. These results can be well explained by taking into account deep-level traps associated with radiation-induced defects.

(2) The experimental results for radiation damage of AlGaAs-GaAs heteroface solar cells have been compared with the theoretical values calculated considering changes in carrier concentrations and minority carrier diffusion lengths due to irradiation. Satisfactory agreement between them shows that the radiation damage in GaAs heteroface solar cells can be evaluated by using radiation damage data in GaAs single crystals.

(3) Numerical analysis is carried out to optimize AlGaAs-GaAs heteroface solar cell structures. Computer calculations show that n^{++}-n^{+}-p heteroface cell structure is more radiation resistant in a solar cell with a shallow junction less than 0.2 μm and a substrate carrier concentration greater than 3×10^{15} cm^{-3}, while p^{++}-p^{+}-n heteroface cell structure is relatively radiation resistant in a deep junction solar cell with a low substrate carrier concentration.

(4) Numerical analysis also shows that optimum window layer thickness for radiation-resistant solar cells is less than 0.1 μm. In the p^{++}-p^{+}-n heteroface solar cell structure, optimum junction depth and substrate carrier concentration are found to be 0.2–0.3 μm and $(2\text{–}5)\times10^{15}$ cm^{-3}, respectively. In the n^{++}-n^{+}-p heteroface solar cell structure, optimum junction depth and substrate carrier concentration are found to be less than 0.1 μm and $(3\text{–}10)\times10^{15}$ cm^{-3}, respectively.

ACKNOWLEDGMENTS

The authors would like to thank K. Matsuyama, H. Takata, T. Kimura, N. Inagaki, and C. Uemura for their valuable suggestions and encouragement.

[1]H. J. Hovel and J. M. Woodall, Appl. Phys. Lett. **30,** 492 (1977).
[2]R. Loo, R. C. Knechtli, and G. S. Kamath, *Proceedings of the IEEE 15th Photovoltaic Specialist Conference* (IEEE, New York, 1981), p. 33.
[3]S. S. Li, *Proceedings of the IEEE 15th Photovoltaic Specialists Conference* (IEEE, New York, 1981), p.27.
[4]S. Yoshida, K. Mitsui, T. Oda, and Y. Yukimoto, Jpn. J. Appl. Phys. **21,** Suppl. 2, 27 (1982).
[5]M. Yamaguchi and C. Amano, J. Appl. Phys. **54,** 5021 (1983).
[6]D. V. Lang, *Radiation Effects in Semiconductors*, Inst. Phys. Conf. Ser. **31,** 70 (1977).
[7]D. Pons, P. M. Mooney, and J. Bourgoin, J. Appl. Phys. **51,** 2038 (1980).
[8]S. S. Li, P. M. Wang, R. Y. Loo, and W. P. Rahilly, Solid State Electron. **26,** 835 (1983).
[9]M. Ettenberg, H. Kressel, and S. L. Gilbert, J. Appl. Phys. **44,** 827 (1973).
[10]V. G. Kustov and V. P. Orlov, Sov. Phys.-Semicond. **3,** 1457 (1970).
[11]K. L. Ashley and J. R. Biard, IEEE Trans. Electron Devices **ED-14,** 429 (1967).
[12]J. Jastrzebski, J. Lagowski, and H. C. Gatos, Appl. Phys. Lett. **27,** 537 (1975).
[13]H. Takakura and Y. Hamakawa, Trans. Inst. Electr. Eng. Jpn. C **36,** 273 (1978) (in Japanese).
[14]A. Onton, *Advances in Solid State Physics* (Pergamon, New York, 1973), Vol. 13, p.59.
[15]J. I. Pankove, *Optical Processes in Semiconductors* (Prentice-Hall, Englewood Cliffs, N.J., 1971), p.35.
[16]A. M. Sekela, D. L. Feucht, and A. G. Milnes, IEEE Trans. Electron Devices **ED-24,** 373 (1977).
[17]A. Yoshikawa and H. Kasai, J. Appl. Phys. **52,** 4345 (1981).